AN EXPERIMENTAL DEMONSTRATION OF NPID CONTROL WITH APPLICATION TO OPTICAL STORAGE DRIVES

Marcel Heertjes * **Frank Cremers** *
Maarten Steinbuch **

* *Philips Applied Technologies, P.O.Box 218, SAQ-1137 / 1128, Eindhoven, The Netherlands*
marcel.heertjes@philips.com / f.l.m.cremers@philips.com
** *Eindhoven University of Technology, P.O.Box 513, W-hoog 0.141, Eindhoven, The Netherlands*
m.steinbuch@tue.nl

Abstract: The application of NPID, or nonlinear PID, control is demonstrated experimentally on an optical storage playback device (CD drive) for automotive applications. The nonlinear design aims at improved shock suppression under equal noise response. This is done by introducing variable controller gains. Namely under large levels of low-frequency vibration, the controller gains are increased as to improve low-frequency sensitivity. High-frequency sensitivity, however, remains unaltered as to keep a low-level noise response.

Keywords: Absolute stability, industrial control, nonlinear control, optical storage devices, performance evaluation

1. INTRODUCTION

Nonlinear control techniques in motion control systems exposed to a wide but generally unknown range of disturbances often lack a significant level of industrial application. In terms of additional control design freedom, this is surprising given the potential of nonlinear control schemes applied to generally linear systems like optical storage drives, see also Yokoyama, *et al.* (1994). Typically in portable or automotive applications, additional control design freedom can be used to improve performance under vibration, e.g. road or engine excitation, but not to deteriorate noise response in the presence of disc scratches or fingerprints. To this end, a nonlinear control scheme based on NPID control is proposed.

NPID control refers to variable controller gains in a PID-based controller structure, see for example Armstrong, *et al.* (2001). In this paper, a controller scheme is presented where the controller gains related to the integral part are increased beyond a pre-defined level for the servo error signals. By doing so, large error signals induced by large levels of vibration are handled more effectively under equal noise response. In the absence of vibrations, small error signals induce no increase in controller gains and therefore are handled equally effective. In terms of design limitations, improved disturbance rejection is temporarily balanced with deteriorated stability margins.

For the purpose of organization, first the NPID control design is presented within the framework of absolute stability theory. Second the implementation of this design on a CD drive is discussed. Third, a performance analysis is presented via measurement under vibration or disc defects. Fourth, an epilogue is given.

2. NPID CONTROL DESIGN

The NPID control scheme such as proposed in this paper refers to the servo control of an objective lens in radial direction, see Fig. 1. In this section,

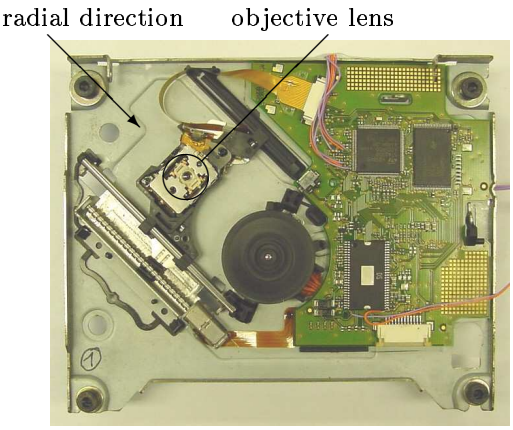

Fig. 1. Bare CD drive.

first the lens dynamics in radial direction are considered, second, the controller design is discussed in terms of nonlinear dynamic filtering, third the nonlinear closed loop dynamics are presented, and, fourth, stability of these nonlinear dynamics are studied in terms of absolute stability.

2.1 Objective lens dynamics

The uncontrolled objective lens dynamics are based on a simple model of the plant P, or

$$\mathrm{P}\,(s) = \frac{\omega_{\mathrm{lp},1}}{(\mathrm{m}\ s^2 + \mathrm{b}\ s + \mathrm{k})(s + \omega_{\mathrm{lp},1})}, \qquad (1)$$

with $s \in \mathbb{C}$ the Laplace variable. The first part of this model contains the objective lens mass m= 1.5 10^{-4} kg along with the mechanical properties of the lens support, i.e. damping b= 2.2 10^{-2} N.s.m^{-1}, and stiffness k= 21.3 N.m^{-1}. The second part represents a first order low-pass filter with $\omega_{\mathrm{lp},1} \approx$ 6.2 10^4 rad.s^{-1}. This is related to actuator inductance in the transfer from voltage to current; see also Bittanti *et al.* (2002).

2.2 NPID controller

Based on radial error measurement, the objective lens dynamics are controlled using a NPID controller. That is, a PID-based filter C_1 having a constant gain in parallel connection with a PI-based filter C_2 having a variable gain ϕ. The choice for the controller structure, in particular the choice for the variable gain part, is driven by nonlinear closed loop stability. This will be motivated in terms of absolute stability theory. But first, the NPID control scheme is considered.

2.2.1. Constant gain PID-based filter The constant gain PID-based filter C_1 is given by

$$\mathrm{C}_1\,(s) = \ \mathrm{k_p}\,(\mathrm{PI}\,(s) + \mathrm{PD}\,(s))\,\mathrm{LP}\,(s), \qquad (2a)$$

with $\mathrm{k_p}$= 2.7 10^3 Nm^{-1} the radial loop gain, PI a lag filter defined by

$$\mathrm{PI}\,(s) = \frac{\gamma\ \omega_{\mathrm{lag}}}{s + \omega_{\mathrm{lag}}}, \qquad (2b)$$

with γ = 20 and ω_{lag}= 8.4 10^1 rad.s^{-1}, a lead filter given by

$$\mathrm{PD}\,(s) = 1 + \frac{s}{\omega_{\mathrm{d}}}, \qquad (2c)$$

with ω_{d}= 1.9 10^3 rad.s^{-1}, and a second order low-pass filter given by

$$\mathrm{LP}\,(s) = \frac{{\omega_{\mathrm{lp},2}}^2}{s^2 + 2\beta\ \omega_{\mathrm{lp},2}\ s + {\omega_{\mathrm{lp},2}}^2}, \qquad (2d)$$

with $\omega_{\mathrm{lp},2}$= 4.4 10^4 rad.s^{-1} and $\beta = 1.1$.

2.2.2. Variable gain PI-based filter The variable gain PI-based filter represents a series connection of a nonlinear part ϕ and a linear part C_2, of which ϕ is given in time-domain by

$$\phi(e_{\mathrm{r}}(t)) = \begin{cases} \alpha\epsilon(e_{\mathrm{r}}(t))(1 - \delta/|e_{\mathrm{r}}(t)|), \text{if } |e_{\mathrm{r}}(t)| > \delta, \\ 0, \ \text{if } |e_{\mathrm{r}}(t)| \le \delta, \end{cases} \qquad (3a)$$

with

$$\epsilon(e_{\mathrm{r}}(t)) = \begin{cases} 1, \ \text{if } |e_{\mathrm{r}}(t)| \ge \delta, \\ 0, \ \text{if } |e_{\mathrm{r}}(t)| < \delta, \end{cases} \qquad (3b)$$

$\alpha > 0$ representing a limit value for the variable gain and δ a dead zone length, see Fig. 2, whereas

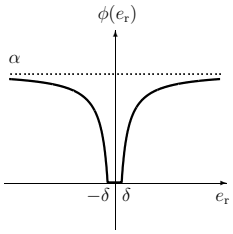

Fig. 2. Graphical representation of inequality (3a).

C_2 is given in frequency domain by

$$\mathrm{C}_2\,(s) = \ \mathrm{k_p}\mathrm{N}\,(s)\,\mathrm{PI}\,(s)\,\mathrm{LP}\,(s), \qquad (4a)$$

with

$$\mathrm{N}\,(s) = \frac{s^2 + 2\beta_1\ \omega_{\mathrm{n},1}\ s + {\omega_{\mathrm{n},1}}^2}{s^2 + 2\beta_2\ \omega_{\mathrm{n},1}\ s + {\omega_{\mathrm{n},1}}^2}, \qquad (4b)$$

representing a notch filter with $\omega_{\mathrm{n},1} \approx$ 1741 rad.s^{-1}, $\beta_1 = 0.2$, and $\beta_2 = 4.1$. In terms of nonlinear closed loop stability, N is designed to enable large values for α. This will be explained hereafter.

2.3 Nonlinear closed loop lens dynamics

The nonlinear closed loop lens dynamics are depicted in Fig. 3 in block diagram representation. It can be seen that the radial error signal e_r being the difference between reference r and objective lens position output y_r forms the input to both

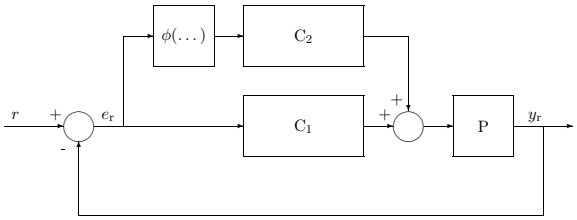

Fig. 3. Nonlinear closed loop lens dynamics.

the constant filter C_1 and the variable gain ϕ.

2.4 Absolute stability of the closed loop

Absolute stability of the nonlinear closed loop lens dynamics are studied using

$$S_c(s) = \frac{C_2(s)\,P(s)}{1 + C_1(s)\,P(s)}. \quad (5)$$

That is, given a class of nonlinearities, stability of the nonlinear feedback connection boils down to Lyapunov stability of the stable linear closed loop dynamics S_c under nonlinear perturbation; see for example Leonov, *et al.* (1996) for conditions imposing stability.

For the considered closed loop lens dynamics, absolute stability is guaranteed if

$$\Re\{S_c(j\omega)\} > -\frac{1}{\alpha},\ 0 \le \omega \le \infty. \quad (6)$$

The graphical interpretation of this inequality is shown in Fig. 4. It requires that S_c remains to

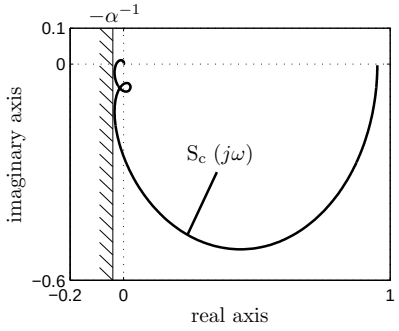

Fig. 4. Graphical interpretation of inequality (6).

the right of a vertical line through the point $(-1/\alpha, 0)$ which is satisfied for values $\alpha < 21.9$. In terms of improved shock suppression, this offers the possibility of having additional low-frequency disturbance rejection (≤ 27.2 dB) resulting from increased controller gain $1 + \alpha$.

3. IMPLEMENTATION ASPECTS

Regarding the proposed nonlinear control scheme, implementation aspects are presented by considering, first, the experimental environment, second, the need for down sampling given a discrete-time controller representation, and, third, a brief model validation by means of measurement.

3.1 Experimental environment

Apart from issues like data acquisition and processing, the experimental environment mainly concerns the experimental setup and the discrete-time controller implementation.

3.1.1. Experimental setup The setup is depicted in Fig. 5. It consists of a bare CD drive, an

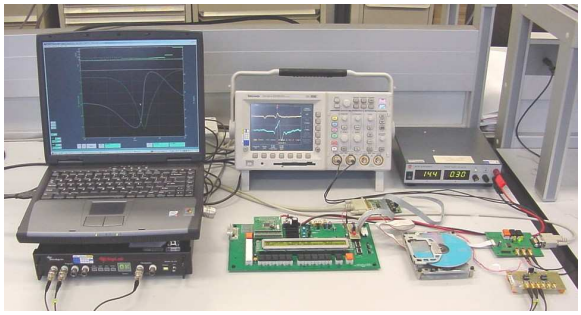

Fig. 5. Experimental setup.

interface to flash (compiled) source code into the micro controller, an interface to adapt the controller parameters once flashed and to designate desired servo signals, an IO-board for monitoring these signals and providing the means to inject noise in the servo loop, and a SigLab/MatLab combination for signal processing and generation.

3.1.2. Discrete-time controller implementation The controller is implemented in discrete time on a DSP chip. To deal with word-size effects in the filter parameters under 16-bit conversion, a parallel configuration is used. That is, the filters PD and LP are evaluated at a sampling frequency of $f_s = 90$ kHz whereas the filters PI and N are evaluated at a down-sampled frequency of 5625 Hz, hence one sixteenth of f_s.

3.2 Down sampling

To illustrate the need for down sampling to improve the controller implementation, the discrete implementation of the notch filter N, see Eq. (4b), is considered in z-domain, or

$$N(z) = \frac{b_0 + 2b_1 z^{-1} + b_2 z^{-2}}{1 + 2a_1 z^{-1} + a_2 z^{-2}}, \quad (7)$$

see Table 1 for the coefficients.

Table 1. Digital notch filter coefficients.

Coefficients	$f_s/16 = 5625$ Hz	$f_s = 90$ kHz
b_0	0.4718	0.9300
b_1	-0.4235	-0.9263
b_2	0.4176	0.9229
a_1	-0.4235	-0.9263
a_2	-0.1107	0.8530

Given a sampling frequency of $f_s = 90$ kHz, it can be seen that the coefficients tend to one, a process that continues for increasing f_s. For a 16-bit conversion in a fixed interval between [-1,1], this induces steady-state output error due to word-size effects in the coefficients, the so-called coefficient quantization error, see Fig. 6. As a consequence, the discrete filter does not

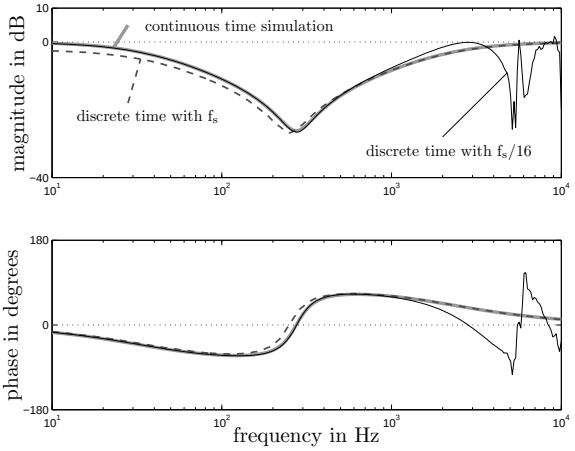

Fig. 6. Bode diagrams of the notch filter in continuous-time simulation and discrete-time implementation. The latter with $f_s = 90$ kHz and down sampled to 5625 Hz, respectively.

show the desired low-frequency behavior, hence the kind of behavior for which it is designed to achieve nonlinear stability and performance. By down sampling of the notch filter input (but also the lag filter input) to $f_s/16 = 5625$ Hz, the low-frequency behavior is significantly improved; see Table 1 for the coefficients. But now the high frequency behavior is affected. This, however, has no consequences for the overall controller performance because N is used in series with PI which has no significant contribution in the high-frequency range; see Eq. (4a).

Besides improved controller implementation, down sampling is used to pre-filter the radial error signal. Namely information is still available on a time scale dictated by the sampling frequency $f_s = 90$ kHz. By taking the average input value over 16 time samples, high-frequency noise is filtered out.

3.3 Model validation in the presence of time delay

To validate the continuous-time model assumptions, it is important to realize that the implementation features several expressions of time delay. An example of which is given by the controller

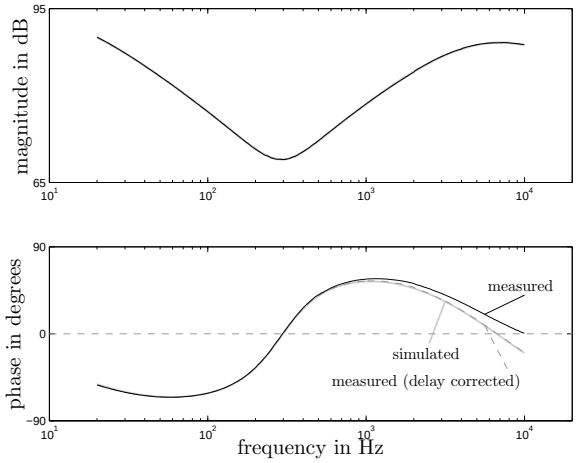

Fig. 7. Bode diagrams of controller transfers with time delay $T_{delay} = 1/(2f_s)$.

characteristics $C_1(j\omega)$ such as depicted in Fig. 7. Here the measured frequency response is based on an input, i.e. the radial error signal, which is monitored as a digital signal and which is converted to the analogue domain via electronic means. The output, however, is monitored directly as an analogue signal. As a consequence, it can be seen that a time delay of $T_{delay} = 1/(2f_s)$ seconds occurs between measurement and simulation.

Another example of time delay is given by the open loop characteristics, see Fig. 8 where a time delay of $T_{delay} = 2/f_s$ seconds is needed to correct the simulations for a proper resemblance with the measurements. The occurrence of time delay

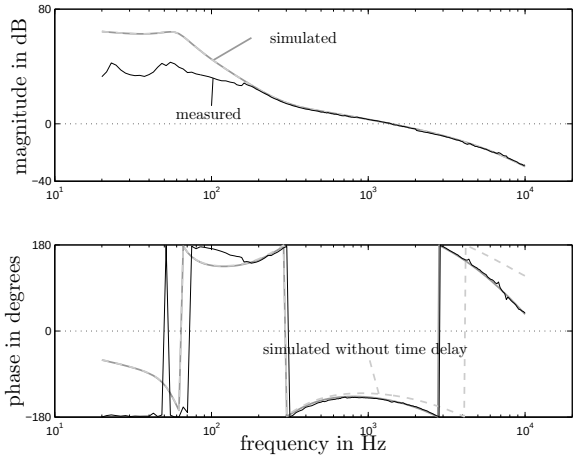

Fig. 8. Bode diagrams of open loop transfers showing a bandwidth of 1.4 kHz, phase margin of 35 degrees, and gain margin of 7.5 dB.

in the implementation has minor impact on the nonlinear closed loop stability result and therefore is neglected in the nonlinear control design.

Apart from time delay, it can be seen in Fig. 8 that below 10 kHz, the sampling frequency of 90 kHz

enables a sufficient match between the continuous-time model and the discrete-time implementation. Below 150 Hz, however, a poor measurement quality is obtained due to the disturbance rejection properties of the control design, hence all measurements are done under closed loop conditions.

4. PERFORMANCE ASSESSMENT

Performance of the nonlinear control design is assessed (with $\alpha = 10$), first, regarding its steady-state behavior under vibration and, second, regarding its transient behavior under disc defects.

4.1 Performance under vibration

To quantify performance under vibration - for automotive applications typically having frequency contents in the range between 10 and 200 Hz - the nonlinear system response is studied at various levels of harmonic excitation. Herein the parameter $\Delta = \delta/\xi$ being the ratio between the dead zone length and the amplitude of excitation is used to characterize shock dependency.

4.1.1. Time-series servo error measurement Fig. 9 shows measured time-series shifted in time of the scaled radial error signal under different levels of disturbance. That is, the periodic radial error

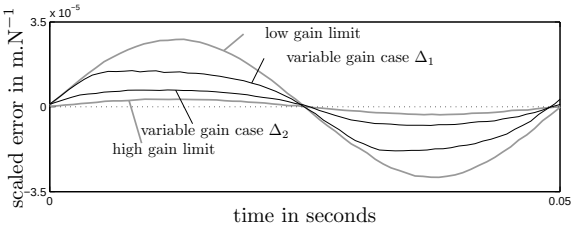

Fig. 9. Time-series measurements (averaged) for $\phi = 0$, $\phi = 10$, and Δ_1 and $\Delta_2 = \Delta_1/2$.

response scaled with the amplitude of a 20 Hz harmonic excitation force, the latter being applied to the objective lens mass. Clearly the control design possesses shock dependency. For small enough amplitudes of excitation, the radial error signals do not exceed the dead zone length giving the low gain linear response $\phi = 0$. For increased levels of disturbance (indicated with Δ_1 and $\Delta_2 = \Delta_1/2$) the dead zone length is exceeded which reduces the response in amplitude and which ultimately induces the high gain linear limit $\phi = 10$.

4.1.2. Nonlinear sensitivity measurement Shock dependency in a broader frequency range is studied in the nonlinear process sensitivity amplitude characteristics of Fig. 10. For the linear limit situations of low gain versus high gain, respectively,

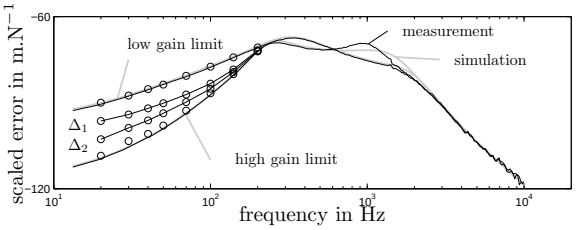

Fig. 10. Process sensitivity analysis for $\phi = 0$, $\phi = 10$, and Δ_1 and Δ_2; measurements together with simulations.

this boils down to the frequency radial error response under force excitation which is given both measured and simulated. For the intermediate levels of disturbance indicated with Δ_1 and Δ_2, the nonlinear frequency response representation is obtained by depicting the maximum absolute value of the scaled periodic radial error response at specific frequencies of harmonic excitation, i.e. the amplitudes in Fig. 9 (Heertjes & Steinbuch, 2004).

In terms of shock suppression, it can be seen that large low-frequency vibration is handled more effectively by the nonlinear control design than small vibration. At low frequencies up to ≈ 21 dB of improvement is obtained. This is not heavily compromised for at high frequencies, hence the considered process sensitivity beyond 2 kHz largely remains unaffected under additional gain. However open loop stability is affected, the phase margin drops from 35 degrees in the absence of variable gain to 22 degrees for the high gain limit.

Though expected to be positively influenced the relation between improved shock suppression and low-level noise response versus the ability to read/write data, expressed for example by the so-called block error rate, is not immediately deduced.

4.2 Performance under disc defects

To evaluate nonlinear performance under disc defects, two types of artificial defects are studied: black dots and fingerprints (Vidal *et al.*, 2001).

4.2.1. Black dot measurement A time-series measurement crossing an 800 μm black dot (grey interval) is shown in Fig. 11. Three different controller settings are depicted: the original low-gain limit, the high-gain limit, and a case of variable gain. During the occurrence of the black dot, the radial error signals equal zero. Beyond the black dot, the response only shows marginal differences in terms of fundamental frequency contribution, rising time, overshoot, and damping properties. This is related to the high-frequency sensitivity properties of the nonlinear control design for which the system is designed to achieve perfor-

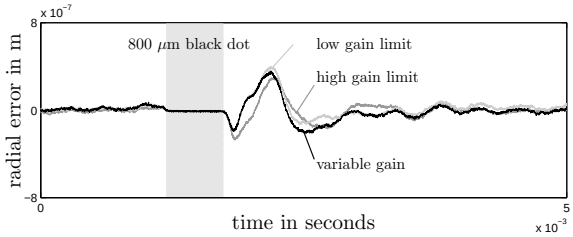

Fig. 11. Time-series measurement (averaged, $\alpha = 10$) crossing an 800 μm black dot.

mance, see Fig. 10. For larger values of α, the differences will be more pronounced.

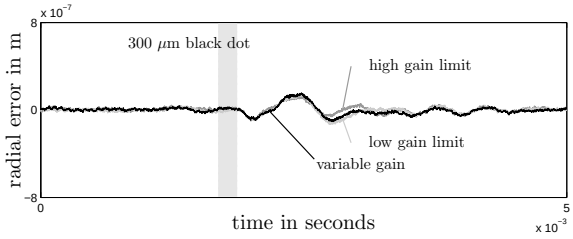

Fig. 12. Time-series measurement (averaged, $\alpha = 10$) crossing a 300 μm black dot.

Similar behavior is shown for the time-series measurements crossing a 300 μm black dot such as depicted in Fig. 12.

4.2.2. Fingerprint measurement A time-series measurement crossing a 20 mm artificial fingerprint is shown in Fig. 13. Apart from the considered radial error signals depicted in the lower part, the focus error signal for the low gain limit is depicted in the upper part. It can be seen that the focus error signal is more sensitive to the fingerprint disturbance than the radial error signal, a fact that is used to monitor its time of exposure. For the considered controller settings, the radial response shows no significant difference.

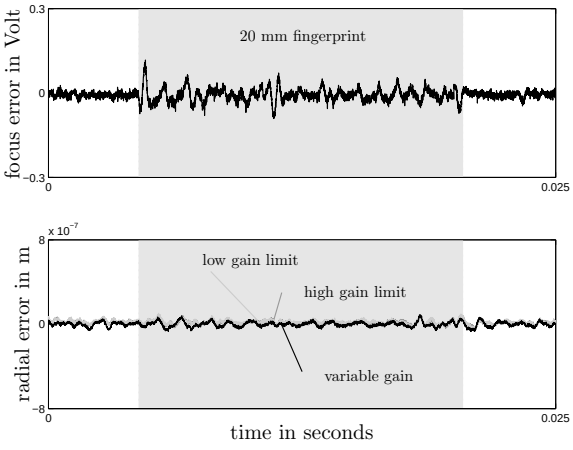

Fig. 13. Time-series measurement (eight times averaged, $\alpha = 10$) crossing a 20 mm fingerprint.

From both the black dot and fingerprint measurements, it is concluded that the nonlinear control design does not induce significant performance deterioration under the considered disc defects, a fact which certainly does not hold true, for example, by increasing the overall controller gain.

5. EPILOGUE

As a means to improve linear system performance by nonlinear control, this paper demonstrated the possibility of NPID control to obtain improved shock performance in optical storage drives under equal noise response. In terms of shock performance, the proposed NPID control scheme shows shock dependency, i.e. the ability to adapt to different disturbance situations. Hereto a temporary increase in shock performance is balanced over a temporary decrease in stability margins. In terms of noise response, the NPID control design does not show significant performance deterioration under black dot and artificial fingerprint disturbance, hence the kind of high-frequency deterioration otherwise occurring under increased overall controller gain, see for example Heertjes & Steinbuch (2004). This is because the nonlinear part of the controller does not contribute to the high-frequency controller output.

REFERENCES

Armstrong, B., D. Neevel and T. Kusid (2001). New results in NPID control: tracking, integral control, friction compensation and experimental results. *IEEE Transactions on Control Systems Technology*, **9**(2), pp. 399–406.

Bittanti, S., F. Dell'Orto, A. Di Carlo and S.M. Savaresi (2002). Notch filtering and multirate control for radial tracking in high-speed DVD-players. *IEEE Transactions on Consumer Electronics*, **48**(1), pp. 56–62.

Heertjes, M.F. and M. Steinbuch (2004). Stability and performance of a variable gain controller with application to a DVD storage drive. *Automatica*, **40**(4), pp. 591–602.

Leonov, G.A., D.V. Ponomarenko and V.B. Smirnova (1996). *Frequency-domain methods for nonlinear analysis - theory and applications*. World Scientific, Singapore.

Vidal, E., P. Andersen, J. Stoustrup and T.S. Pedersen (2001). A study on the surface defects of a compact disk. In *Proc. IEEE Conference on Control Applications*, pp. 101–104. Mexico, Mexico city.

Yokoyama, E., M. Nagasawa and T. Katayama (1994). A disturbance suppression control system for car-mounted and portable optical disk drives. *IEEE Transactions on Consumer Electronics*, **40**(2), pp. 92–99.